Hindawi
Geofluids
Volume 2022, Article ID 8793136, 18 pages
https://doi.org/10.1155/2022/8793136

Research Article

Factors Controlling the Hydraulic Fracture Trajectory in Unconventional Reservoirs

Peng Zheng,[1,2] **Erhu Liu**,[3] **Desheng Zhou**,[2] **Xinwei Du**,[2] **and Zhongjun Ma**[4]

[1]*Xi'an University of Science and Technology, Xi'an, 710054 Shaanxi, China*
[2]*College of Petroleum Engineering, Xi'an Shiyou University, Xi'an, 710065 Shaanxi, China*
[3]*Gas Production Plant 2 of Yanchang Gasfield, Shaanxi Yanchang Petroleum (Group) Co., Ltd., Jingbian, China*
[4]*No. 1 Gas Production Plant, Yanchang Petroleum Group Exploration Company, Yan'an, 716000 Shaanxi, China*

Correspondence should be addressed to Peng Zheng; 1183678063@qq.com and Desheng Zhou; desheng@xsyu.edu.cn

Received 21 April 2022; Accepted 26 May 2022; Published 11 July 2022

Academic Editor: Hao Wu

The morphology of hydraulic fracture is affected by many factors. In previous studies, due to the heterogeneity of rock samples and the limitations of sample size, influence degree of various factors on fracture deflection angle has not been well distinguished in laboratory experiments. Based on the boundary element method, we established a mathematical model to study the factors controlling the morphology of hydraulic fracture. Simulation results show that with increasing injection pressure, the radius of the fracture curvature increases. When the difference between the injection pressure and the maximum principal stress is 5 times the ground stress difference, the influence of in situ stress on hydraulic fracture deflection can be ignored. Hydraulic fracture deflection angle was relatively larger when considering the viscosity of the fracturing fluid. When stress difference is too small or the injection pressure is too big, the deflection angle of fracture is easy to fluctuate during initial propagation. Too large Young's modulus and too small Poisson's ratio will inhibit the fracture deflection and cause a narrower width of fracture. The effect of Poisson's ratio on fracture aperture is less than 1 mm. When perforation angle is perpendicular to maximum horizontal principal stress, the fracture width first increases rapidly and then gradually decreases from heel to tip. The influence degree of each factor on fracture deflection is ranked: stress difference of in-situ stress is the biggest, followed by injection pressure and perforation angle. This study is of great significance for the control of hydraulic fracture morphology and the further improvement of fracturing effect.

1. Introduction

With the progress of science and technology, people's demand for energy grew with the passage of time [1–3]. From 2010 to 2019, global consumption of natural gas increased by 23.5%, while oil is 12.7%. By 2020, fossil fuel consumption accounts for 90% of the world primary energy consumption (24.7% natural gas and 31.2% oil) [4]. Currently, unconventional oil and gas reserves are abundant, but due to its low flow capacity [5–8], hydraulic fracturing technology is an important way to enhance oil and gas recovery on unconventional reservoir [9–12].

Since the introduction and application of hydraulic fracturing technology in previous decades, extensive research has been conducted on the damage of rock, propagation and evolution of hydraulic fracture (HF), migration of hydraulic fracturing proppant. The propagation of HF is always the focus of field engineers [13–17]. Due to lack of accurate and effective monitoring technology, it is impossible to directly observe the HF propagation process and morphology of underground reservoir [18]. Many scholars have studied the initiation and propagation of HF by numerical simulation method and laboratory-scale fracturing experiments.

In experiments, Xing et al. studied the influence of loading rate on the size of fracture process zone through the Brazil splitting test [19]. Experiment results have shown that with the loading rate increasing, the length of fracture process zone increased from about 5 mm to 17 mm. Fast fluid injection inhibits the deflecting of NF (natural

fracture), allowing HF to propagate along the initially designed direction [20]. Yang et al. used dynamic caustics in conjunction with high-speed photography to investigate the interaction of running fractures by obliquely incident blast stress waves, which revealed that the moving fracture intended to deflect away from the blast wave source when the fracture and stress wave have the same direction; however, it will propagate toward the blast wave source when they have opposite direction [21]. In the initial stage of hydraulic fracturing, HF is dominated by tensile failure, while compression and shear events tend to occur in the nonplanar extension stage [22]. Due to the limitation of sample size, physical experiments are often difficult to quantitatively reflect the crack trajectory under the influence of multiple factors.

Therefore, numerical simulation techniques are widely used to study and predict hydraulic fracture propagation trajectories. At present, the investigation of the deflection rule during HF propagation always focus on the effect of injection pressure and rate, maximum horizontal principal stress, perforation angle, etc. Zheng et al. [23] proposed that during the propagation of HF, it was easier to deflect to the side of the high pore pressure area. Zhao et al. [24] simulated the influence of injection rate and perforation angle on fracture propagation. With the increase of perforation angle and injection rate and decrease of stress difference, HF tend to propagate in the original direction and turning distance from well increase. Zhou et al. and Zheng et al. [25, 26] proposed H factor to evaluate the combined effect of in situ stress, injection pressure, and perforation angle; however, they did not make a parallel comparison of the influence of each factor. Meanwhile, various damage criteria have been used in simulation model, such as energy release rate criterion [27], maximum circumferential stress criterion [28], and minimum strain energy density criterion [29]. Physically, the maximum energy release rate is the most acceptable. But so far, it is difficult to explain the fracture path observed in the experiment, and there is still no unified result. The two-dimensional model based on strain energy density is in good agreement with the experimental results. However, the physical nature of the connection between the theory and material destruction remains unclear. Compared with the above two fracture criteria, maximum circumferential stress criterion is more suitable for brittle fracture problems. When the perforation direction during hydraulic fracturing is not perpendicular to the horizontal minimum principal stress direction, HF is subjected to both tensile stress (by injected fluid into the fracture) and shear stress (by in situ stress), which will deflect in the direction of the maximum principal stress [25, 30].

As is known to all, the trajectory of hydraulic fractures is often affected by formation heterogeneity, which makes it difficult to reach the target fracture length or create complex fracture networks. Therefore, controlling hydraulic fractures to stimulate natural fractures to produce complex fracture networks or to communicate multiple oil-gas enrichment areas is an important way to improve fracturing effects. The above research provides abundant references for the effective control of HF in field construction but still has some problems that need to be resolved. For example, the influence degree of different factors on fracture deflection has not been quantitatively compared, the morphology of hydraulic fractures in 3-dimensional view is studied, and few people have studied the change of fracture deflection trajectory caused by rock mechanical properties.

To reveal the mechanism of HF deflection during propagation, based on the theory of linear elasticity and fracture mechanics, a numerical simulation model with boundary element method was established. This paper is organized as the following 3 sections. The construction of the computational model and relevant validation are described in Section 2. Parametric studies are presented in Section 3 to analyze fracture morphology and curvature radius during propagation. The paper ends with some conclusions in Section 4.

2. Numerical Model

2.1. Model Assumption. In reality, the propagation of hydraulic fracture is the result of the joint action of multiple physical fields. At present, it is difficult to establish a multifield coupling solution model considering the interaction of all factors. So in order to simplify the calculation model and focus our research on fracture morphology and stress interference in horizontal well, the following assumptions are introduced during the establishment of the mathematical model: (1) the target formation belongs to linearly elastic medium; (2) HF satisfies the plane strain condition [31]; (3) the study domain is infinite and ignores the abnormal pressure caused by geological tectonic movement; (4) the fracture propagation process follows the theory of linear elastic fracture mechanics [32]; (5) the fluid inside the HF is incompressible and belongs to the Poiseuille flow between two parallel plates [33]; and (6) this paper does not consider proppant migration and uneven distribution within the fracture.

2.2. Fracture Deformation and Flow of Fracturing Fluid in Fracture. Displacement discontinuity method (DDM) is one of the boundary element methods (BEM) and first proposed by Crouch [34]. In this paper, we use DDM to simulate the deformation of HF and induce stress field. Separate HF into N segment discontinuous microelements. When a discrete fracture microelement is subjected to field stress in the discrete state, relative displacement between the upper and lower surfaces will occur. In general, the shear stress and normal stress in each element of fracture is as follows [35]:

$$\begin{cases} \sigma_s^i = \sum_{j=1}^{N} A_{ss}^{i,j} D_s^j + \sum_{j=1}^{N} A_{sn}^{i,j} D_n^j \\ \sigma_n^i = \sum_{j=1}^{N} A_{ns}^{i,j} D_s^j + \sum_{j=1}^{N} A_{nn}^{i,j} D_n^j \end{cases} (i, j = 1, 2, \cdots, N), \quad (1)$$

where D_s, D_n are the horizontal and vertical relative displacements of the discontinuous microelement in s–n coordinate system, m; $A_{ss}^{j,i}, A_{sn}^{j,i}, A_{nn}^{j,i}, A_{ns}^{j,i}$ are the influence

coefficients of unit i under the discontinuous displacement of unit j, Pa/m; and σ_s^i, σ_n^i are the shear stress and normal stress in fracture element, respectively, Pa. The impact coefficients are as follows:

$$\begin{cases} A_{ss}^{i,j} = 2G\left[-f'^{\bar{x}\bar{y}} \sin 2\gamma - f'^{\bar{y}\bar{y}} \cos 2\gamma - \bar{y}\left(f'^{\bar{x}\bar{y}\bar{y}} \sin 2\gamma - f'^{\bar{y}\bar{y}\bar{y}} \cos 2\gamma\right)\right], \\ A_{sn}^{i,j} = 2G\left[-\gamma\left(f'^{\bar{x}\bar{y}\bar{y}} \cos 2\gamma + f'^{\bar{y}\bar{y}\bar{y}} \sin 2\gamma\right)\right], \\ A_{nn}^{i,j} = 2G\left[2f'^{\bar{x}\bar{y}} \sin^2\gamma + f'^{\bar{y}\bar{y}} \sin 2\gamma - \bar{y}\left(f'^{\bar{x}\bar{y}\bar{y}} \cos 2\gamma + f'^{\bar{y}\bar{y}\bar{y}} \sin 2\gamma\right)\right], \\ A_{ns}^{i,j} = 2G\left[-f'^{\bar{y}\bar{y}} + \bar{y}\left(f'^{x\bar{y}\bar{y}} \sin 2\gamma - f'^{\bar{y}\bar{y}\bar{y}} \cos 2\gamma\right)\right], \end{cases} \tag{2}$$

where f'^{x}, f'^{y}, f'^{xx}, f'^{xy}, f'^{xyy}, and f'^{yyy} are the derivatives of function $f(x, y)$, respectively; ν is the Poisson ratio; and G is the shear modulus, MPa. For a detailed description of rock deformation, refer to our previous studies [36].

In the initial stage of fracturing, the HF is affected by both in situ stress and fluid pressure inside the fracture. Considering that the study domain is infinite, the stress equilibrium equation on each fracture element is given by

$$\begin{cases} \sigma_s^i = -\dfrac{1}{2}(\sigma_h - \sigma_H) \sin 2\beta^i \\ \sigma_n^i = p_i - \sigma_h \sin^2\beta^i - \sigma_H \cos^2\beta^i \end{cases} \quad (i = 1, 2, \cdots, N), \tag{3}$$

where σ_h, σ_H are the minimum and maximum horizontal in situ stress, Pa, and β^i is the angle between the X-axis and the s^i-axis in ith element, rad.

Navier-Stokes equations are introduced to describe the pressure drop of the fracturing fluid in HF. At this point, the flow of power-law fluid on a flat plate between two smooth planes can be expressed as [37]

$$\frac{\partial p(x,t)}{\partial x} = -2^{\ddot{n}+1} k \left(\frac{1+2n}{\ddot{n}}\right)^{\ddot{n}} \frac{1}{w^{2\ddot{n}+1}} \frac{q}{h_f} \left|\frac{q}{h_f}\right|^{\ddot{n}-1}, \tag{4}$$

where P is the pressure inside the fracture, Pa; q is the flow rate per unit time through the fracture cross section, m^3/s; h_f is the height of HF, m; w is the width of fracture, m; and $\ddot{n}$ and k are the fluid power law index and the consistency index, respectively. In general, fracturing fluid is Newtonian fluid, so $\ddot{n} = 1$:

$$q(x,t) = -\frac{h_f w^3}{12k} \frac{\partial p}{\partial x}. \tag{5}$$

Put Equations (1) and (3) into a matrix form:

$$\begin{bmatrix} \overline{A_{ss}} & \overline{A_{sn}} \\ \overline{A_{ns}} & \overline{A_{nn}} \end{bmatrix} \begin{bmatrix} \overline{D_s} \\ \overline{D_n} \end{bmatrix} = \begin{bmatrix} \overline{\sigma_s} \\ \overline{\sigma_n} \end{bmatrix}. \tag{6}$$

By eliminating $\overline{D_s}$ in Equation (7), the width of HF ($\overline{D_n}$) can be directly solved:

$$\overline{A_{ns}} \cdot \overline{A_{ss}}^{(-1)} \cdot \overline{\sigma_s} - \overline{A_{ns}} \cdot \overline{A_{ss}}^{(-1)} \cdot \overline{A_{sn}} \cdot \overline{D_n} + \overline{A_{nn}} \cdot \overline{D_n} - \overline{\sigma_n} = 0, \tag{7}$$

where

$$\begin{aligned} \overline{A_{sn}} &= \begin{bmatrix} A_{sn}^{11} & A_{sn}^{12} & \cdots & A_{sn}^{1N} \\ A_{sn}^{21} & A_{sn}^{22} & & A_{sn}^{2N} \\ \vdots & & \ddots & \vdots \\ A_{sn}^{N1} & A_{sn}^{N2} & \cdots & A_{sn}^{NN} \end{bmatrix}, \\ \overline{D_s} &= \begin{bmatrix} D_s^1 \\ D_s^2 \\ \vdots \\ D_s^N \end{bmatrix}, \\ \overline{A_{ns}} &= \begin{bmatrix} A_{ns}^{11} & A_{ns}^{12} & \cdots & A_{ns}^{1N} \\ A_{ns}^{21} & A_{ns}^{22} & & A_{ns}^{2N} \\ \vdots & & \ddots & \vdots \\ A_{ns}^{N1} & A_{ns}^{N2} & \cdots & A_{ns}^{NN} \end{bmatrix}, \\ \overline{A_{nn}} &= \begin{bmatrix} A_{nn}^{11} & A_{nn}^{12} & \cdots & A_{nn}^{1N} \\ A_{nn}^{21} & A_{nn}^{22} & & A_{nn}^{2N} \\ \vdots & & \ddots & \vdots \\ A_{nn}^{N1} & A_{nn}^{N2} & \cdots & A_{nn}^{NN} \end{bmatrix}, \\ \overline{D_n} &= \begin{bmatrix} D_{\mathrm{n}}^1 \\ D_n^2 \\ \vdots \\ D_n^N \end{bmatrix}, \\ \overline{\sigma_s} &= \begin{bmatrix} -\dfrac{1}{2}(\sigma_h - \sigma_H) \sin 2\theta_1 \\ -\dfrac{1}{2}(\sigma_h - \sigma_H) \sin 2\theta_2 \\ \vdots \\ -\dfrac{1}{2}(\sigma_h - \sigma_H) \sin 2\theta_N \end{bmatrix}, \\ \overline{\sigma_n} &= \begin{bmatrix} p_{f1} - \sigma_h \sin^2\theta_1 - \sigma_H \cos^2\theta_1 \\ p_{f2} - \sigma_h \sin^2\theta_2 - \sigma_H \cos^2\theta_2 \\ \vdots \\ p_{fN} - \sigma_h \sin^2\theta_N - \sigma_H \cos^2\theta_N \end{bmatrix}. \end{aligned} \tag{8}$$

Then, the specific stresses and displacements of each point in the reservoir caused by jth microelements can be obtained as follows [11]:

$$\begin{cases} u^j{}_x = D_{\bar{x}}\left[2(1-\nu)f'^{\bar{y}} - yf'^{\bar{x}\bar{x}}\right] + D_{\bar{y}}\left[-(1-2\nu)f'^{\bar{x}} - yf'^{\bar{x}\bar{y}}\right], \\ u^j{}_y = D_{\bar{x}}\left[2(1-\nu)f'^{\bar{x}} - yf'^{\bar{x}\bar{y}}\right] + D_{\bar{y}}\left[2(1-\nu)f'^{\bar{y}} - yf'^{\bar{y}\bar{y}}\right], \\ \sigma^j{}_{xx} = 2GD_{\bar{x}}\left(2f'^{\bar{x}\bar{y}} + yf'^{\bar{x}\bar{y}\bar{y}}\right) + 2GD_{\bar{y}}\left(f'^{\bar{y}\bar{y}} + yf'^{\bar{y}\bar{y}\bar{y}}\right), \\ \sigma^j{}_{yy} = 2GD_{\bar{x}}\left(-yf'^{\bar{x}\bar{y}\bar{y}}\right) + 2GD_{\bar{y}}\left(f'^{\bar{y}\bar{y}} + yf'^{\bar{y}\bar{y}\bar{y}}\right), \\ \sigma^j{}_{xy} = 2GD_{\bar{x}}\left(f'^{\bar{y}\bar{y}} + yf'^{\bar{x}\bar{y}\bar{y}}\right) + 2GD_{y}\left(-yf'^{\bar{y}\bar{y}\bar{y}}\right), \end{cases} \tag{9}$$

where $\sigma^j{}_{xx}, \sigma^j{}_{yy}, \sigma^j{}_{xy}, u^j{}_x, u^j{}_y$ are the induced stress and displacements.

2.3. The Initiation and Propagation of Fracture. The stress intensity factors (SIFs) are important parameters to describe the field stress of fracture tip, which is calculated by discontinuous displacement value on the fracture surface. SIFs at the fracture tip can be shown [38]:

$$\begin{cases} K_I = \dfrac{0.806E\sqrt{\pi}}{4(1-\upsilon^2)\sqrt{2a}}D_n, \\ K_{II} = \dfrac{0.806E\sqrt{\pi}}{4(1-\upsilon^2)\sqrt{2a}}D_s, \end{cases} \tag{10}$$

where K_I and K_{II} are the stress intensity factor of different types of cracks, MPa•m$^{0.5}$; E is Young's modulus, MPa; ν is Poisson's ratio; and a is the half-length of crack, m.

At the same time, the maximum circumferential stress (MCS) criterion is introduced to judge the initiation and propagation direction of fracture [39]. The fracture deflection angle can be obtained by solving the first-order partial derivative for the circumferential stress:

$$\theta_0 = \arcsin\left[\frac{K_{II}\left(K_I + 3\sqrt{K_I{}^2 + 8K_{II}{}^2}\right)}{K_I{}^2 + 9K_{II}{}^2}\right]. \tag{11}$$

The mixed mode of stress intensity factor is used to identify the initiation of HF:

$$K_e = \cos\frac{\theta_0}{2}\left[K_I\cos^2\frac{\theta}{2} - \frac{3}{2}K_{II}\sin\theta_0\right], \tag{12}$$

When$K_{\mathrm{IC}} > \mathrm{K}_e$, fracture is initiated. Preset cracks propagate at a fixed length each time.

2.4. Flow Chart. The computer program flow chart (Figure 1) and corresponding solving procedure are as follows: (1) input initial parameters, such as maximum horizontal stress, minimum horizontal stress, Young's modulus, Poisson's ratio, fracture toughness, injection pressure, perforation depth, and perforating angle; (2) hydraulic fracture discretization and establish the deformation equation with Equations (1) and (5); (3) use the Newton-Raphson iteration method to calculate the discontinuous displacement of fracture element, pressure in fracture; (4) check the current construction time and total time; if the total time is reached, finish calculation; (5) if construction time does not reach the total time, calculate the stress intensity factor (Equation (10)) and determine whether the tip of HF has cracked (Equation (12)); (6) calculate the deflection angle (Equation (11)) with maximum circumferential stress [25], and increase the number of fracture element and construction time; (7) go to step 2 again, and make the fracture element discrete. The hydraulic fracture path is built step by step until the construction time is bigger than the total time.

2.5. Model Validation. Firstly, verify the induced stress caused by fracture deformation. Our model satisfies the plane strain condition and assumes that the height of fracture is constant [32]. The analytical solution of the induced field stress around the fracture can be expressed as [40]

$$\begin{cases} \sigma_x = -P_f\dfrac{r}{a}\left(\dfrac{a^2}{r_1r_2}\right)^{3/2}\sin\theta\sin\left[\dfrac{3}{2}(\theta_1+\theta_2)\right] - P_f\left[\dfrac{r}{\sqrt{r_1r_2}}\cos\left(\theta - \dfrac{\theta_1+\theta_2}{2}\right) - 1\right], \\ \sigma_y = P_f\dfrac{r}{a}\left(\dfrac{a^2}{r_1r_2}\right)^{3/2}\sin\theta\sin\left[\dfrac{3}{2}(\theta_1+\theta_2)\right] - P_f\left[\dfrac{r}{\sqrt{r_1r_2}}\cos\left(\theta - \dfrac{\theta_1+\theta_2}{2}\right) - 1\right], \\ \sigma_{xy} = -P_f\dfrac{r}{a}\left(\dfrac{a^2}{r_1r_2}\right)^{3/2}\sin\theta\cos\left[\dfrac{3}{2}(\theta_1+\theta_2)\right], \end{cases} \tag{13}$$

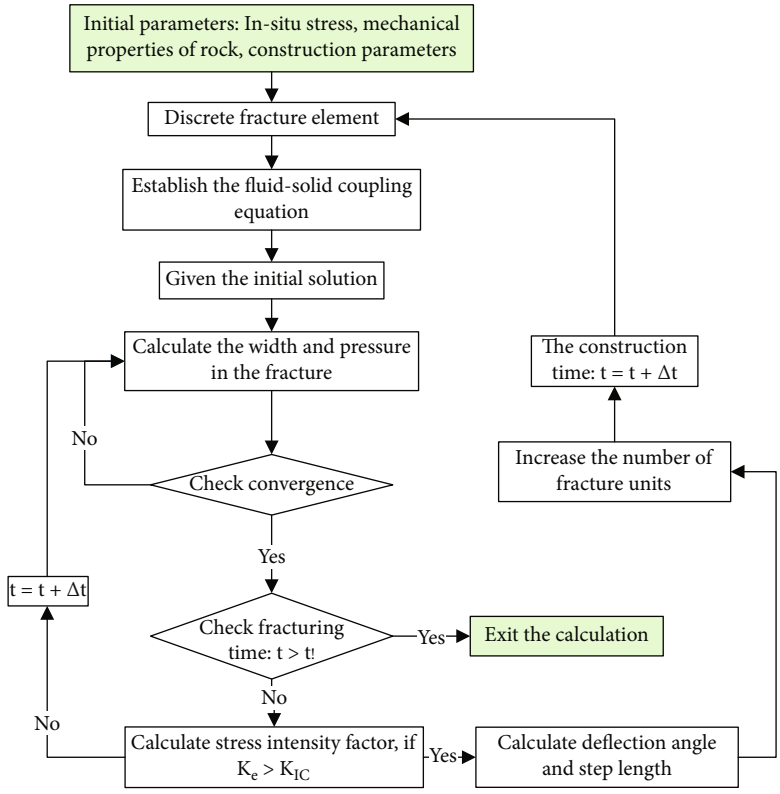

Figure 1: Computer program flow chart.

where P_f is the injection pressure, Pa; r, r_1, r_2 are, respectively, the distance between the fracture and the point Q, m; and θ, θ_1, θ_2 are the angle between the X-axis and the line the distance. The specific mechanical model is shown in Figure 2(a).

The initial simulation parameters are as follows: injection pressure (P_f) is -3 MPa, the half-length of crack (a) is 1 m, the coordinates of point Q: $x = 0.5$ m, and y increase from 0 m to 10 m. Calculate the induced stress at point Q under different vertical distances (coordinate y) from the fracture plane. The normal stress and shear stress obtained by simulation and calculation decrease with the increase of the distance from the fracture plane, and the numerical solution is basically consistent with the analytical solution, where in Figure 2(b), the solid line represent analytical results, and the dotted line represents the simulation results.

Compared with other simulation method and approaches, DDM has some clear advantages. The discretization of the elastic problem reduces to defining the unknowns only on the fracture surface, which significantly lowers the size of the problem. At the same time, the elasticity equations can be constructed easily due to the stresses along the fracture which are equal to the superposition of the contribution of discontinuity displacement on all fracture elements. Besides this, deformation equation, which derived from analytic solution, makes the calculation result have high precision.

3. Results and Discussion

3.1. The Distribution of Induced Stress after Hydraulic Fracturing. The purpose of this paper is to quantitatively assess the influence degree of different factors on the deflection of HF. Our numerical simulation is primarily aimed at unconventional reservoirs, so the simulation data are mainly based on the rock mechanical parameters of unconventional reservoirs. The algebraic relationships among perforating angle, deflection angle, in situ stress, and injection pressure are established based on previous studies [25].

$$\begin{aligned}\left(H + \cos^2\beta\right)\sin\theta &= \frac{1}{2}\sin 2\beta(3\cos\theta - 1),\\ H &= \frac{P_f - P_H}{P_H - P_h},\end{aligned} \tag{14}$$

where θ is the deflection angle and β is the perforating angle.

However, in the derivation of the basic model, it is assumed that HF is straight line, so the above equation cannot be used for the calculation of continuous fracture deflection. And the superposition effects of other hydraulic fracture elements on fracture tip elements should also be considered. Therefore, numerical simulation is carried out based on the boundary element method. The fracture trajectory and the influence of fracture deformation on horizontal principal stress distribution are shown in Figure 3. A

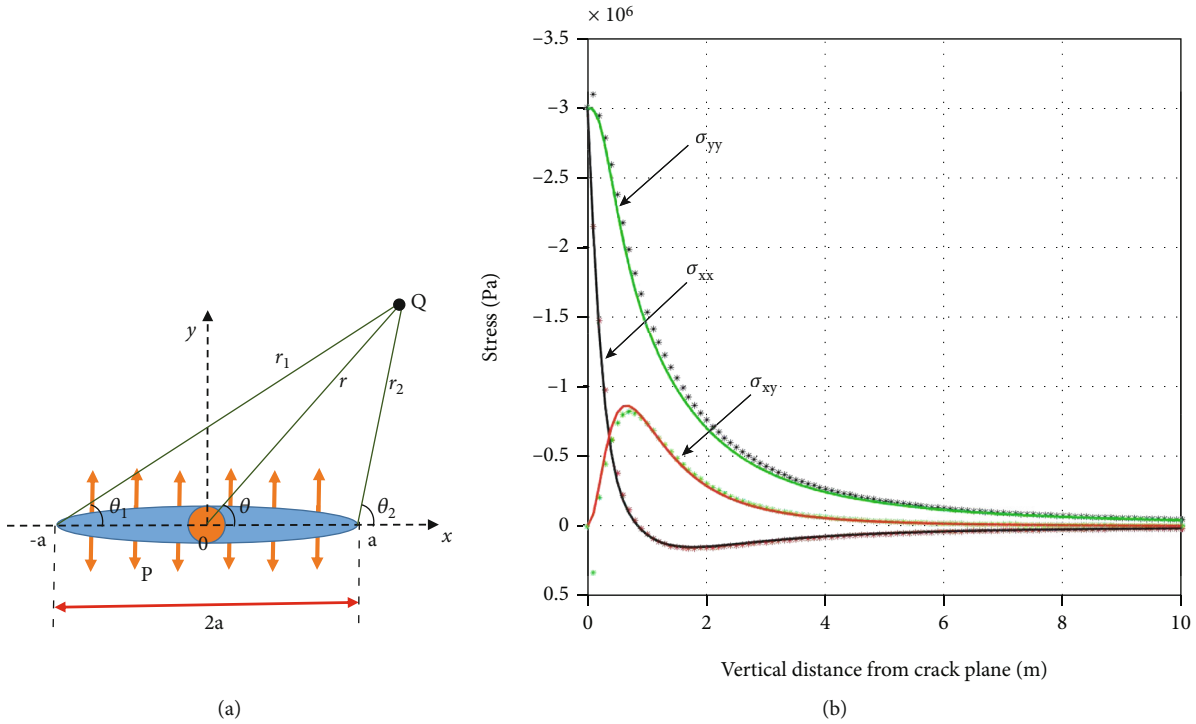

FIGURE 2: Computer program flow chart: (a) mechanical model; (b) comparison of simulation results; "∗" represents the numerical solution. Solid lines represent analytical solutions.

schematic diagram is provided in Figure 3(a)to indicate the boundary conditions and the initial fracture location compared to the reservoir. The initial parameters are as shown in Table 1.

From Figures 3(b) and 3(c), we can see that under in situ stress, fractures tend to deflect to maximum horizontal stress direction. The planar-induced stress distribution can be intuitively shown in Figures 3(b) and 3(c). However, the force magnitude and the positive and negative sign of the force in the fracture tip area determine the subsequent propagation direction of the fracture. Therefore, Figures 3(d) and 3(e) are drawn to show the magnitude and direction of stress. In this paper, when the normal stress is positive, it means the reservoir is under tension, and vice versa. Shear stresses always occur in pairs; they are equal and opposite. During the propagation of HF, tensile stress areas are formed on both tips of the fracture. At the same time, the abrupt change of shear stress at the crack tip indicates that the shear stress also affects HF deflection.

3.2. The Deflection of Hydraulic Fracture. Construction parameters and rock mechanics parameters are often important factors affecting fracture deflection. So we will discuss the deflection mechanism of hydraulic fracture from injection pressure (P_f), horizontal principal stress (σ_h, σ_H), perforating angle, viscosity of fracturing fluid (μ), and mechanical properties of rock (E, ν) and finally determine the degree of influence of different factors on fracture deflection. The simulation data is shown in Table 2. These data are applicable to tight sandstone reservoirs, and we have summarized the value range of data in previous studies. For details, please refer to Zheng et al. [36]. According to formula (14), there is a certain relationship between stress difference and HF angle. Therefore, in order to make each parameter have comparability between each other, the study of the in situ stress and the pressure in the fracture is expressed in the form of stress difference.

In our simulation, ignore fracturing fluid filtration. On the premise of given injection pressure, only the pressure drop of fracturing fluid under the condition of flat flow in the fracture is considered. In order to make the fracture have more deflection space for easy observation, the basic direction of the fracture is approximately perpendicular to the maximum horizontal principal stress. The maximum horizontal principal stress was set as a constant value (40 MPa) so that other stress values could be determined. The perforating depth is 1 m, the initial perforating angle of fracture is defined as the angle between the perforation direction and the maximum horizontal stress direction. Note that in a homogeneous reservoir, when the fracture is completely perpendicular to the direction of maximum horizontal principal stress, the fracture does not deflect due to the zero cosine value, but this does not occur in a real reservoir due to reservoir heterogeneity. Therefore, in order to better fit the actual situation, when the perforation angle is 90°, we will set a small tilt in the model so that the cosine is very small but not zero.

We divided the simulation into 12 groups and set groups 3 and 10 as the control group, to study the influencing factors of HF deflection, including horizontal principal stress

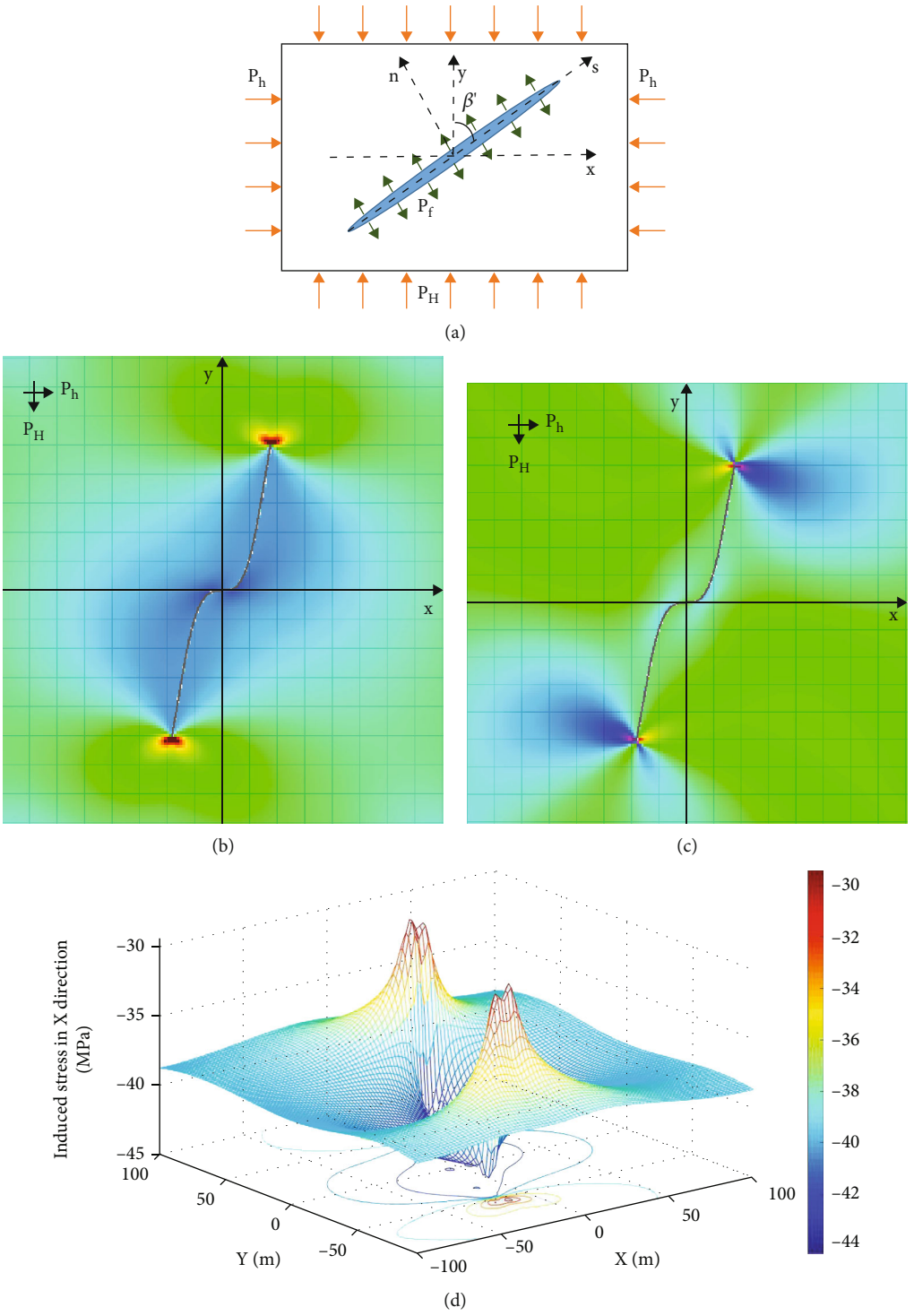

FIGURE 3: Continued.

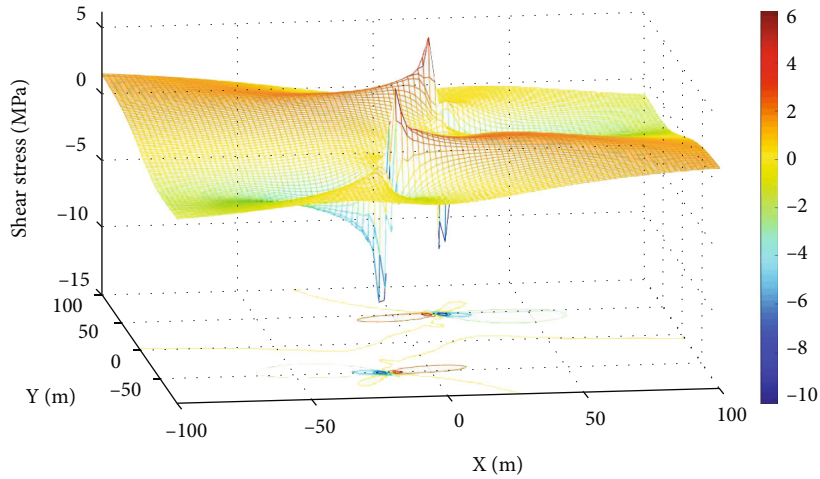

(e)

Figure 3: Hydraulic fracture morphology and induced stress field: (a) initial crack location and stress model; (b) normal stress σ_{xx}; (c) shear stress σ_{xy}; (d) the fluctuation of σ_{xx} in the simulated region; (e) the fluctuation of σ_{xy} in the simulated region.

Table 1: Data for simulation.

Young's modulus	30 GPa
Poisson's ratio	0.25
Maximum horizontal stress	40 MPa
Minimum horizontal stress	38 MPa
Injection pressure	43 MPa
Perforating depth	1 m
Fracture toughness (MPa·m$^{1/2}$)	2.5 MPa·m$^{1/2}$

difference (cases 1-3), hydraulic fracture pressure (cases 3-5), differences in initial perforating angle (cases 3, 6, and 7), the pressure inside hydraulic fracture considering the fluid pressure drop (cases 8-10), the viscosity of fracturing fluid with the pressure drop in the fracture (cases 10-12), and consider and disregard fluid pressure drop (cases 5 and 10). To eliminate the effect of fluid pressure reduction during fracture deflection, the pressure was set constant in the simulation to allow a complete analysis and comparison of simulation results from the perspective of single factor influence. The simulation results of first seven groups are as shown in Figure 4. From cases 1 to 3, we can see that with the decrease of the minimum horizontal principal stress, the interference effect of stress difference on fracture deflection gradually increases. It can be predicted that if the direction of in situ stress reverses in the later period, the fracture track will swing back and forth, and the swing amplitude will increase with the increase of the stress difference. Cases 3-5 show that the greater the internal pressure of hydraulic fracture is, the easier it is for the fracture to get rid of the influence of in situ stress on its track direction in the process of propagation. Cases 3, 6, and 7 indicate that the direction of perforation has a great influence on the hydraulic fracture trajectory. When the hydraulic fracture extends along the approximate horizontal principal stress direction, the influence of the maximum horizontal principal stress on the hydraulic fracture trajectory increases gradually. Xing et al. [20] proposed the influence of injection rate on fracture deflection; the increase in injection rate is similar to the increase in injection pressure in cases 3-5. But their research did not involve the effect of stress difference, perforation angle, fracturing fluid viscosity, etc.

In order to have a clear exhibition of the morphology of HF in three-dimensional view during hydraulic fracturing, we constructed the pseudo-three-dimensional morphology about the torsion of HF by orthogonally superimposing the plane strain model. Specifically, the fracture propagation morphology in the X-Z plane is calculated first, and then, the fracture propagation morphology is calculated for each node element mentioned above in the X-Y plane with the coordinates of each node element as the starting point. Finally, the fracture plane is constructed by interpolation. In this paper, the X-axis is the direction of minimum horizontal principal stress, which is also the wellbore direction. The Y- and Z-axes represent the direction of maximum horizontal principal stress and vertical in situ stress, respectively. These two forces are usually perpendicular to the wellbore. Simulation results are as shown in Figure 5. It can be seen from the figure that the greater the pressure in the fracture, the easier the hydraulic fracture is to propagate along its initial direction; on the contrary, the lower the pressure in the fracture, the easier the fracture surface is torsion.

3.3. The Curvature Radius of Hydraulic Fracture during Deflection. In the above section, the deflection morphology of a single fracture is mainly studied, but it did not clearly reflect the deflection rate during HF propagation, and as a result, we cannot evaluate which factors are more likely to cause fracture deflection. Therefore, in this section, the fracture deflection rate is amplified by converting the fracture deflection angle into the radius of curvature. The fracture deflection radius model is shown in Figure 6(a). Suppose

Table 2: Data for simulation.

Case category	Maximum horizontal principal stress (MPa)	Minimum horizontal principal stress (MPa)	Pressure in HF (P_f) (MPa)	Initial perforating angle (°)	Consider fluid pressure drop (P_f)	Fracturing fluid viscosity (MPa·s)
Case 1 $\Delta P_{H-h} = 1$	40	39	43	90	/	/
Case 2 $\Delta P_{H-h} = 5$	40	35	43	90	/	/
Case 3 control group 1	40	38	43	90	/	/
Case 4 $\Delta P_{f-H} = 4$	40	38	44	90	/	/
Case 5 $\Delta P_{f-H} = 10$	40	38	50	90	/	/
Case 6 $\Delta\beta = 45$	40	38	43	45	/	/
Case 7 $\Delta\beta = 20$	40	38	43	20	/	/
Case 8 P_f	40	38	/	90	46	45
Case 9 P_f	40	38	/	90	43	45
Case 10 control group 2	40	38	/	90	50	45
Case 11 μ	40	38	/	90	50	85
Case 12 μ	40	38	/	90	50	125

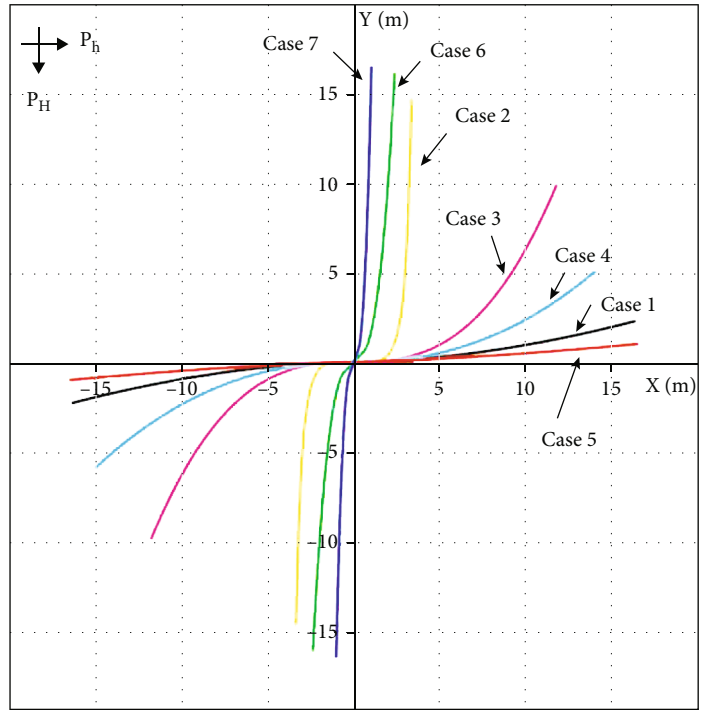

Figure 4: Morphology of hydraulic fracture with different conditions.

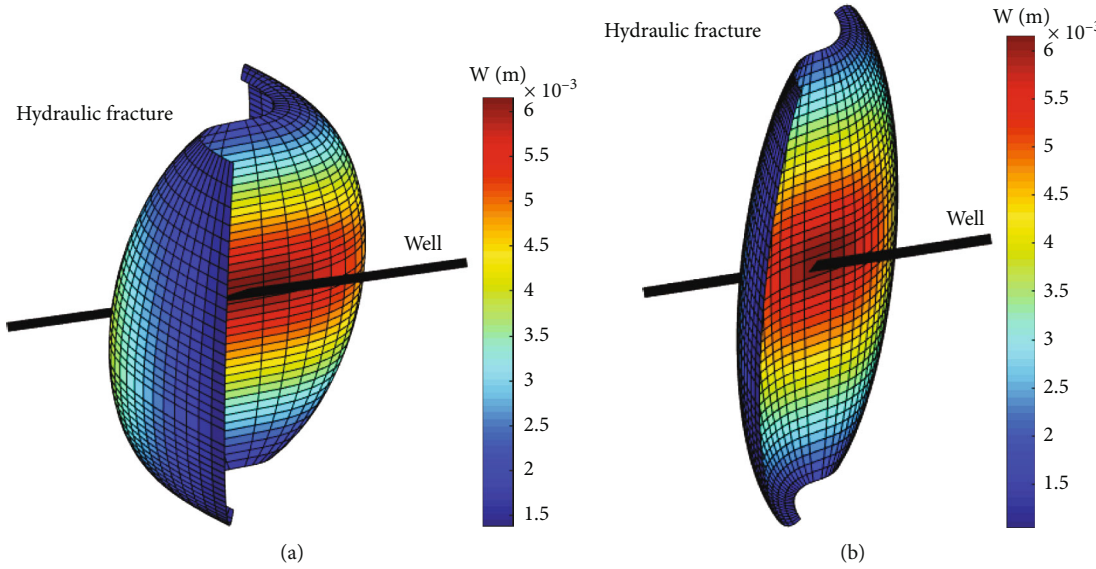

Figure 5: Spatial morphology of hydraulic fractures: (a) case 3; (b) case 5.

that the deflection angle of a discrete fracture element is $\theta_{(r,i)}$; then,

$$\theta_{(r,i)} = \begin{cases} \theta_{i+1} - \theta_i, & i = 1, 2, 3 \cdots n, \\ \theta_1, & i = 1, \end{cases} \tag{15}$$

where θ_i is the angle between HF and the direction of minimum horizontal principal stress.

The curvature radius of each fracture element is calculated. And the deflection rate is as shown in Figure 5(b).

In Figure 6, the slope of the curve can be used to represent the fracture deflection rate. By observing cases 3, 6, and 7 in Figure 6(b), it is found that the deflection of fracture caused by the perforating angle basically tends to be stable after HF propagation of about 3 m; this indicates that the original propagation direction of HF cannot be maintained only by increasing the perforation angle. From cases 1 to 3 in Figure 6(c), we can see that, in the stage of crack

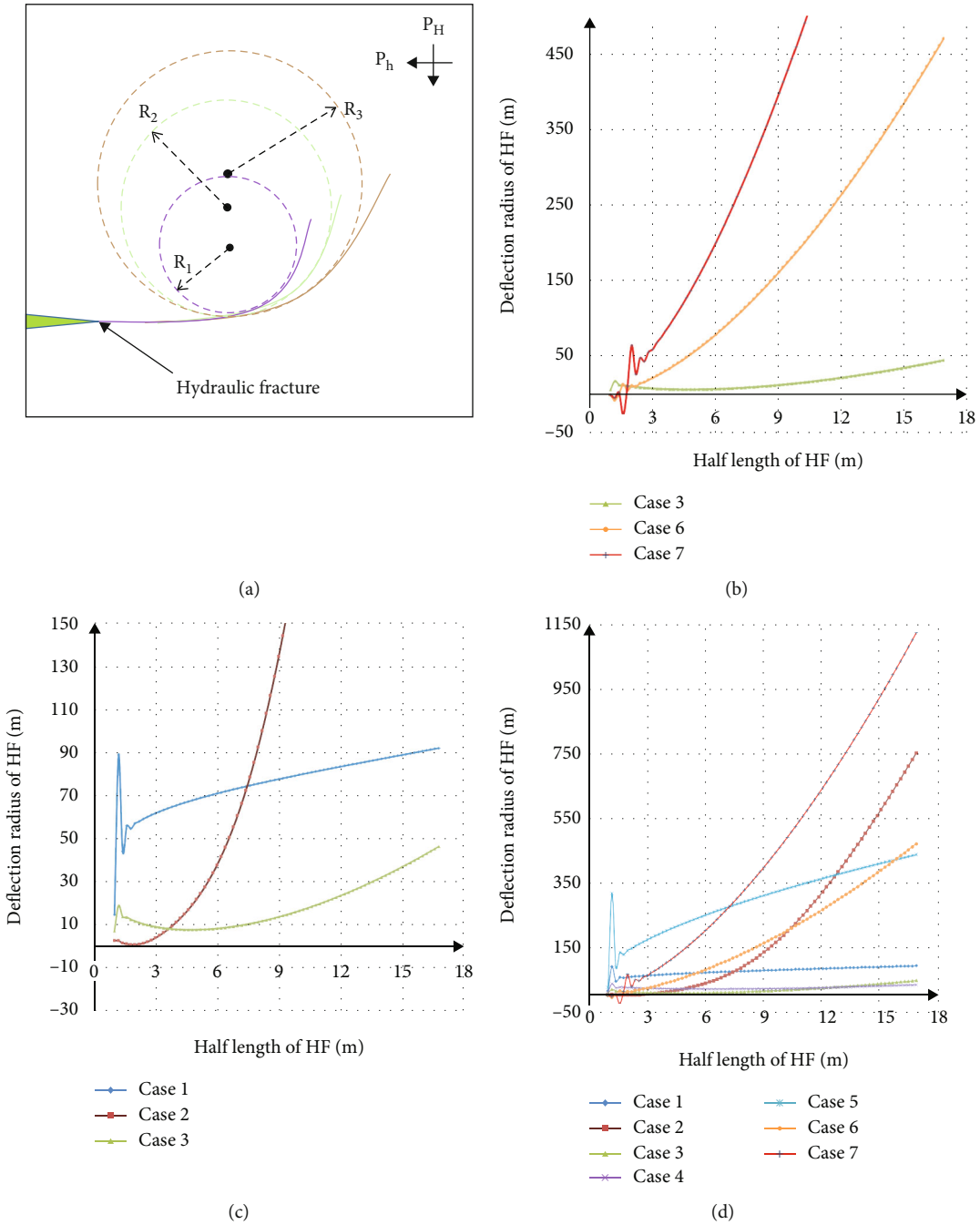

FIGURE 6: The fracture curvature radius. (a) The physical model. R_1, R_2, and R_3 are the curvature radius, respectively. (b) Curvature radius of HF with different perforation angles. (c) Curvature radius of HF with different stress differences. (d) Curvature radius of HF from cases 1 to 7.

initiation, the greater the stress difference, the more likely the crack will be deflected, while the deflection velocity of fracture caused by stress difference gradually accelerates. Since the HF has been deflected a lot in the initial stage, after the HF propagated for 5-10 m, the greater the stress difference, the less likely the crack will be deflected. For comprehensive comparison, we draw the first seven groups of case curves in one graph, Figure 6(d). According to cases 3-5, the influence of fluid pressure inside the HF on the deflection rate is not obvious when it is too low. Only when the pressure in the fracture is much greater than the maximum horizontal principal stress, the deflection rate will decrease significantly, but it is still decreasing gradually, and the curve is convex. When the pressure in the fracture is large enough, the fracture can easily maintain the original extension direction. By comparing the above three factors, the influence degree of each factor on fracture deflection is ranked: stress difference of in situ stress > injection pressure > perforating angle.

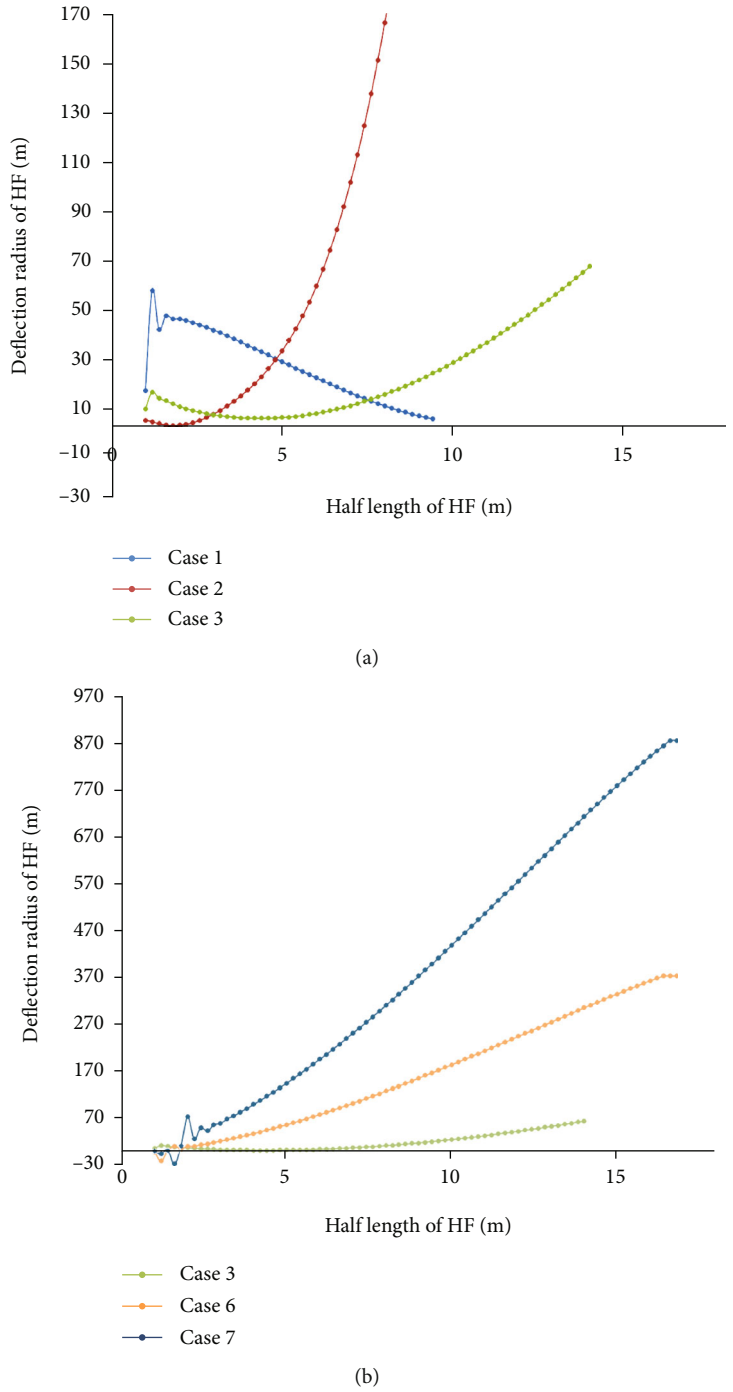

Figure 7: The fracture curvature radius of the HF. (a) Under different stress differences. (b) Under different perforation angles.

The fluctuation of the curve at the initial position is due to the length of the HF which is too small at the initial moment, which causes the HF to be affected by both the in situ stress and the element length. This is the same as the commonly observed saw tooth crack in reality. This phenomenon series is obvious in cases 1, 5, and 7; thus, it can be seen that low stress difference and high injection pressure easily lead to unstable deflection at the initial moment. But it will disappear when the hydraulic fracture reaches 2-9 times of its initial length.

3.4. The Deflection of Hydraulic Fracture considering the Drop of Fluid Pressure. We have studied the deflection of HF without considering the drop of fluid pressure in the above cases (1-7). Now, fluid flow and pressure drop in rock fractures are described by the Navier-Stokes equations in fluid mechanics [37]. For comparison, we simulated the

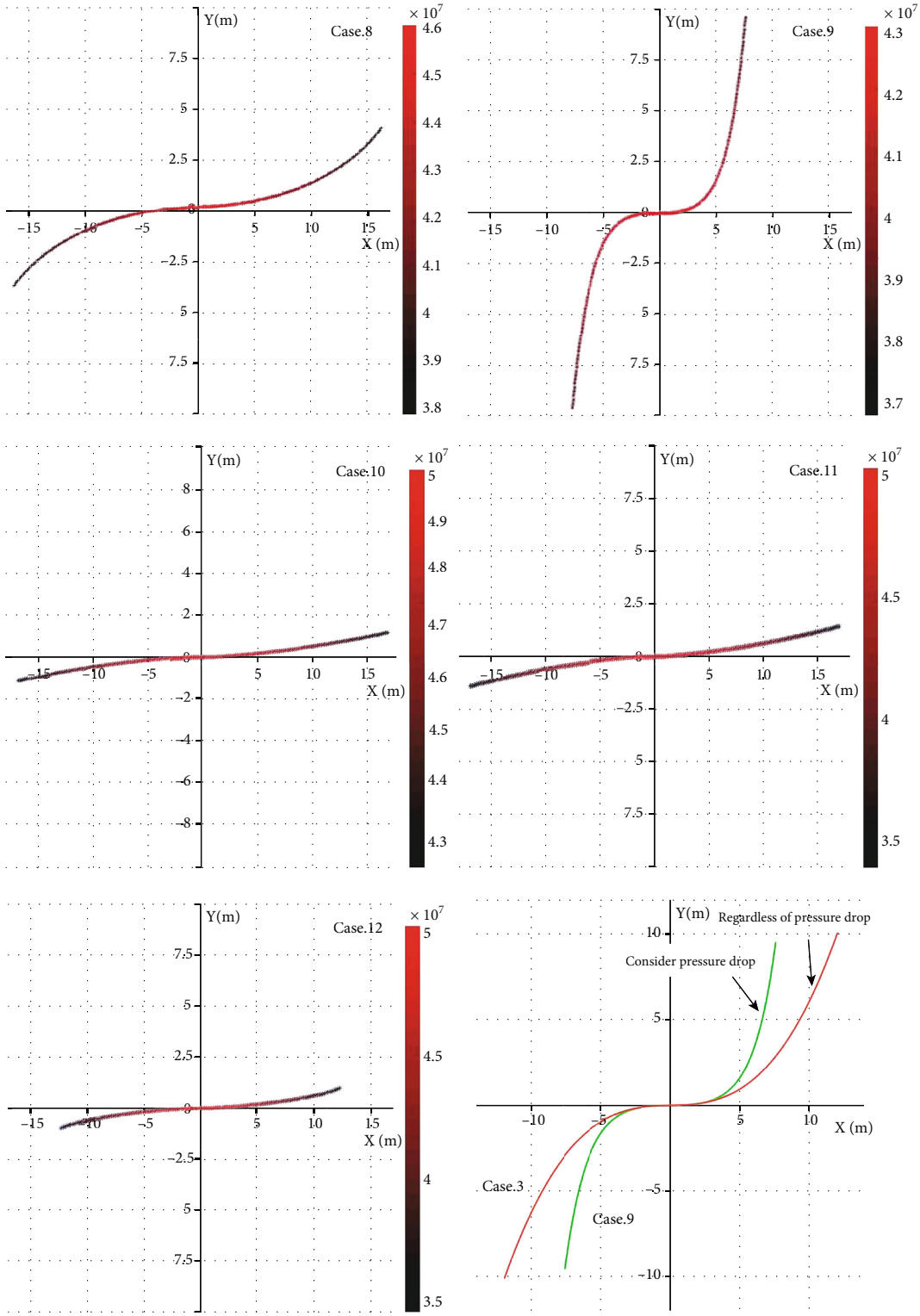

Figure 8: HF morphology when considering the drop of fluid pressure in the HF.

cases 1-3, 6, and 7 to study the deflection situation under different stress differences and perforation angles, which considered the drop of fluid pressure. Figure 7 indicates that fractures can easily stop propagation due to loss of pressure drop. At the same time, the pressure drop loss further

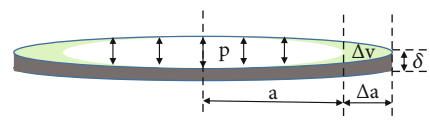

Figure 9: Propagation of HF.

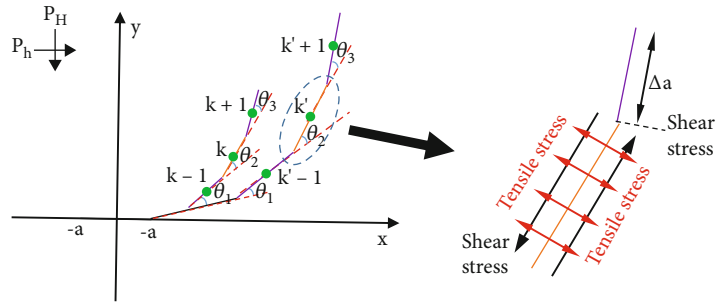

Figure 10: Propagation trajectories of HF under different length increments.

weakens the influence of the perforation angle on the fracture trajectory.

Cases 8-12 in Figure 8 are the simulation results of the effect of fracture pressure and fracturing fluid viscosity on fracture deflection when considering fluid pressure drop.

It can be seen from Figure 8 that the fracture deflection of cases 8-10 in considering the drop of fluid pressure is similar to that without pressure drop. Cases 10-12 indicate that with increasing viscosity of the fracturing fluid, the pressure in the fracture decreased more rapidly, but the deflection angle of HF was relatively inconspicuous. However, the initiation of HF will be suppressed when the viscosity of fracturing fluid is too high (case 12). Thus, the adjustment space to adjust the fracture trajectory through the viscosity of the fracturing fluid was limited. Comparing case 3 with case 9, the fluid pressure drop can cause significant change in fracture trajectory. Reducing the viscosity of fracturing fluid without considering filtrate is helpful for fractures to restrain the influence of in situ stress on its deflection. However, low-viscosity fracturing fluid is more likely to penetrate into the formation, resulting in a faster drop of pressure in the fracture, and excessive fluid viscosity will cause frictional resistance increase and increased pressure loss making it difficult to initiate HF.

3.5. Influence of Rock Mechanical Properties on Fracture Trajectory. We have studied the influence of construction factors on fracture deflection in the above section, and then, we will study the influence of rock mechanical properties on it. It can be seen from the numerical model in Section 2 that, when simulating HF propagation, it is necessary to determine the deflection angle and propagation length of the crack tip each time it breaks. From Equations (1) and (2), we can see that when the crack surface is stressed, it can be written in the following form:

$$D_n = \frac{\mathscr{R}_1}{G}, \quad D_s = \frac{\mathscr{R}_2}{G}, \tag{16}$$

where G is the shear modulus, $G = E/(2(1-\upsilon))$, and $\mathscr{R}_1$ and $\mathscr{R}_2$ are the constant coefficient.

Substitute formula (16) for formula (10):

$$K_I = \frac{\mathscr{R}_3}{1+\upsilon}, \quad K_{II} = \frac{\mathscr{R}_4}{1+\upsilon}, \tag{17}$$

where $\mathscr{R}_3$ and $\mathscr{R}_4$ are the constant coefficient.

It can be seen that the stress intensity factor is independent of Young's modulus in this solving process. From Equations (10), (11), and (17), we can obtain the following relation:

$$\theta_0 = \arcsin\left[\frac{\mathscr{R}_4\left(\mathscr{R}_3 + 3\sqrt{\mathscr{R}_3{}^2 + 8\mathscr{R}_4{}^2}\right)}{\mathscr{R}_3{}^2 + 9\mathscr{R}_4{}^2}\right]. \tag{18}$$

Now, it can be seen that the combination of the previous boundary element deformation equation, the stress intensity factor solution equation, and the maximum circumferential stress criterion is suitable for judging the instability of the fracture tip. However, this method cannot well reflect the influence of rock mechanical properties (E, ν) when calculating the deflection angle and fracture propagation length after fracture tip rupture, so it is not suitable for simulating fracture trajectories under different rock mechanical properties.

Based on the above situation, we introduce Griffith energy release theory [41, 42] to analyze this problem. Suppose that there is an infinitely thin plate of thickness δ; the shape of HF in it is as shown in Figure 9, where P is the fluid pressure in the fracture, Δa is a certain length in fracture tip, and Δv is the volume increment of the fracture after the fracture tip expands for a certain length.

At this time, the work done by the fluid pressure P on the fracture surface can be expressed as ΔW_p, and the work done by the in situ stress is $\Delta W_1 (\Delta W_1 = \Delta \mathrm{v} \bullet \sigma_\mathrm{n})$. As fracture propagates, a part of the energy is converted into strain energy and stored in the rock matrix. This part of the energy can be expressed as ΔW_0, and the remaining energy is used to supply new cracks, which is called the specific surface

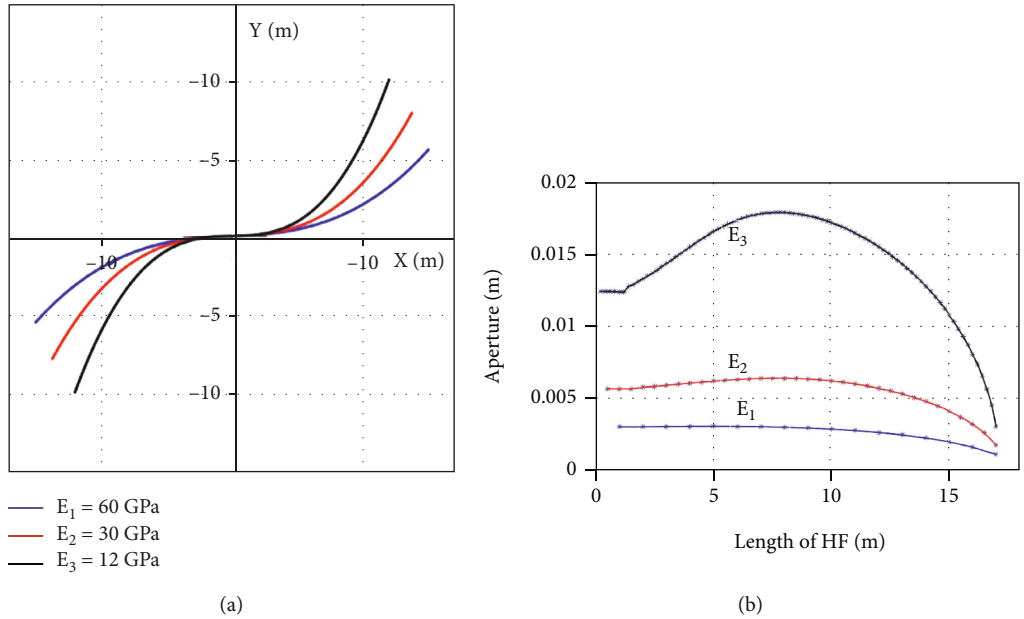

Figure 11: Simulation results with different Young's moduli: (a) fracture morphology; (b) fracture aperture.

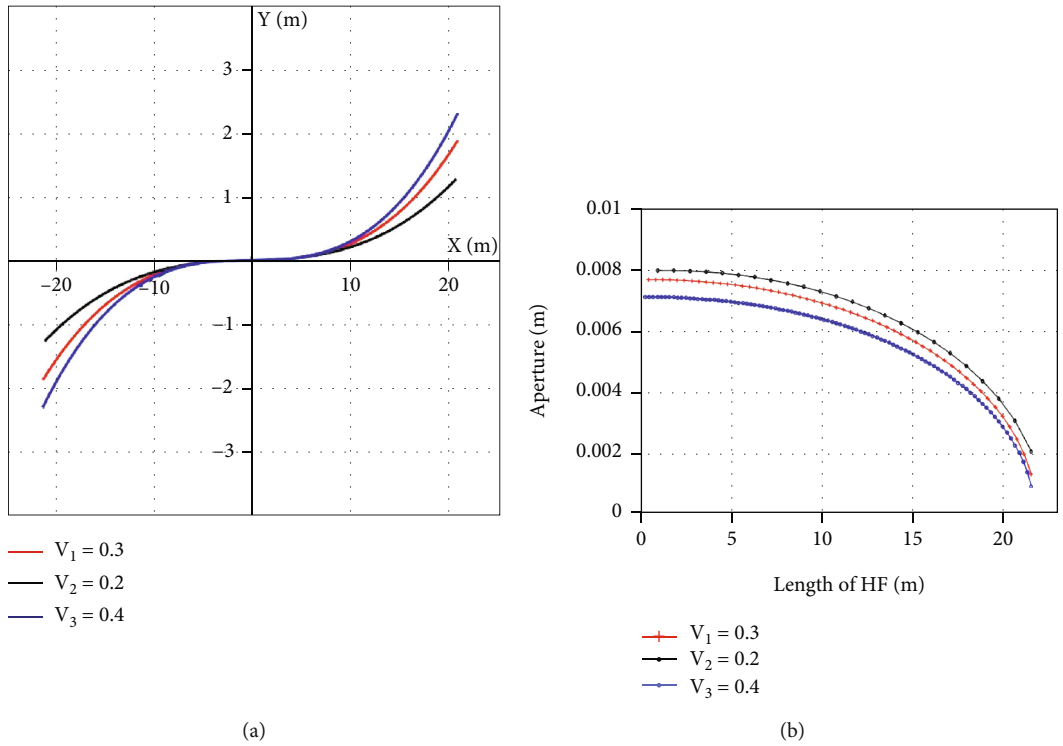

Figure 12: Simulation results with different Poisson's ratios: (a) fracture morphology; (b) fracture aperture.

energy, and its size is $2\gamma\delta\Delta c$. Then, the energy balance equation can be expressed as [43]

$$\Delta W_P = \Delta W_0 + \Delta W_1 + 2\gamma\delta\Delta a. \tag{19}$$

Different rock mechanical properties have different surface energies, so the length increments generated during instability are also different, which will lead to different extension trajectories of fractures, as shown in Figure 10. Under the combined action of tensile stress and shear stress,

even if the fracture element is deflected at the same angle, different propagation paths are produced when the element lengths are different.

At this time, the fracture volume increment can be expressed as [42]

$$\Delta v = 2\pi\delta\sigma_{\mathrm{n}} a \bullet \frac{\Delta a}{E'} = Q_0 \bullet \Delta t, \tag{20}$$

where E' is the modulus of elasticity for plane strain condition, $E' = E/(1-v^2)$; γ is surface energy; δ is the thinness of infinite domain; and Q_0 is the injection rate of the fracturing pump.

When fracturing fluid filtration is not considered, from the volume balance, the fracture volume change is equal to the fluid volume injected per unit time step, so we can obtain the length increment per unit time step at the crack tip. The influence of Young's modulus is as shown in simulation results in Figures 11 and 12. As Young's modulus increases and Poisson's ratio decreases, the fractures are less prone to deflection, and the fracture aperture will be reduced accordingly at the same time. The biggest apertures of HF do not always appear at the wellhead. This is because the initial fracture is approximately perpendicular to the maximum horizontal principal stress. With the deflection of the hydraulic fracture, the compressive stress on the fracture surface from the direction of the maximum principal stress will decrease, and the width of HF will increase relatively. However, as the length of HF continues to increase, the fracture width gradually decreases, and the smaller the Young modulus, the greater the rate of the HF width. Note that this model does not consider the effect of proppant on fracture pressure.

4. Conclusions

In this paper, a fracture deflection model during hydraulic fracture propagation is established to simulate the trajectory of HF under different parameters.

The deflection of HF is affected by different parameters, which include the construction parameters during HF propagation and the geologic parameters. And these parameters contain a compensation relationship. In other words, the influence of the same parameter with different values on the fracture deflection trajectory can be compensated for and balanced by other parameters.

Under the influence of different parameters, the deflection rate of hydraulic fractures is not the same. In order to clearly show the different factors on HF deflection, we used curvature radius to evaluate the deflection rate of HF. Stress difference has the greatest influence on the curvature radius of HF. However, when the pressure in hydraulic fracture is much greater than the horizontal in situ stress, the in situ stress has little influence on the deflection of hydraulic fracture. When stress difference is too small or the injection pressure is too big, the deflection angle of fracture is easy to fluctuate during initial propagation. The influence degree of each factor on fracture deflection is ranked: stress difference of in situ stress > injection pressure > perforating angle.

As the fracturing fluid viscosity increases, the pressure in the fracture decreased more rapidly, but the hydraulic fracture deflection angle was relatively larger than the fracture with higher fracturing fluid viscosity. When considering the fluid pressure drop, HF is easier to deflect.

Theoretical analysis shows that conventional methods for coupling boundary element deformation calculation model, stress intensity factor calculation and maximum circumferential stress criterion, cannot distinguish the influence of rock mechanical properties on the deflection of hydraulic fractures during hydraulic fracturing. Based on this situation, a calculation method of the fracture extension increments at the fracture tip based on energy release is introduced in discontinuous displacement model.

As Young's modulus increase and Poisson's ratio decreases, the fractures are less prone to deflection, and the fracture aperture will be reduced accordingly at the same time. The biggest apertures of HF do not always appear at the wellhead; this is often related to the angle between the fracture and the maximum horizontal principal stress.

There are still many shortcomings in this paper. Future studies will be a systematic and in-depth study of fracture morphology under different geological conditions and fracturing technologies. In terms of numerical simulation, optimize the calculation model so that the propagation of three-dimensional fracture can be calculated, and consider the heterogeneity of pore pressure, rock mechanical properties, multiscale cracks, etc. In laboratory experiments, large-scale fracturing experiments will be carried out to verify the simulation results. Finally, we hope to develop a set of hydraulic fracturing methods that can be used for fracture morphology control based on this paper.

Data Availability

All the data have been included in the manuscript.

Conflicts of Interest

The authors declare no conflict of interest.

Acknowledgments

This work was supported by the National Natural Science Foundation of China (51934005, 51874242).

References

[1] A. Azadeh and S. Tarverdian, "Integration of genetic algorithm, computer simulation and design of experiments for forecasting electrical energy consumption," *Energy Policy*, vol. 35, no. 10, pp. 5229–5241, 2007.

[2] G. Aydin, "The application of trend analysis for coal demand modeling," *Energy Sources, Part B: Economics, Planning, and Policy*, vol. 10, no. 2, pp. 183–191, 2015.

[3] Y. Y. Feng and L. Zhang, "Scenario analysis of urban energy saving and carbon abatement policies: a case study of Beijing

city, China," *Procedia Environmental Sciences*, vol. 13, pp. 632–644, 2012.

[4] B. Petroleum, *Statistical review of world energy*, BP, London, 2021.

[5] M. J. Mayerhofer, E. P. Lolon, N. R. Warpinski, C. L. Cipolla, D. Walser, and C. M. Rightmire, "What is stimulated reservoir volume?," *SPE Production & Operations*, vol. 25, no. 1, pp. 89–98, 2010.

[6] H. L. Matthews, G. W. Schein, and M. R. Malone, "Stimulation of gas shales: they're all the same-right?," in *SPE hydraulic fracturing technology conference*, College Station, Texas, USA, 2007SPE 106070.

[7] J. Xu, Z. Chen, and R. Li, "Impacts of pore size distribution on gas injection in intraformational water zones in oil sands reservoirs," *Oil & Gas Science and Technology–Revue d'IFP Energies Nouvelles*, vol. 75, p. 75, 2020.

[8] J. Xu, K. Wu, R. Li et al., "Real gas transport in shale matrix with fractal structures," *Fuel*, vol. 219, pp. 353–363, 2018.

[9] S. Salimzadeh, R. W. Zimmerman, and N. Khalili, "Gravity hydraulic fracturing: a method to create self-driven fractures," *Geophysical Research Letters*, vol. 47, no. 20, 2020.

[10] Y. Zhao, S. Cao, D. Shang et al., "Crack propagation and crack direction changes during the hydraulic fracturing of coalbed," *Computers and Geotechnics*, vol. 111, pp. 229–242, 2019.

[11] X. Chen, J. Zhao, Y. Li, W. Yan, and X. Zhang, "Numerical simulation of simultaneous hydraulic fracture growth within a rock layer: implications for stimulation of low-permeability reservoirs," *Journal of Geophysical Research: Solid Earth*, vol. 124, no. 12, pp. 13227–13249, 2019.

[12] J. Xu, K. Wu, R. Li et al., "Nanoscale pore size distribution effects on gas production from fractal shale rocks," *Fractals*, vol. 27, no. 8, p. 1950142, 2019.

[13] D. Zhou and P. He, "Major factors affecting simultaneous frac results," in *SPE Production and Operations Symposium*, Oklahoma City, Oklahoma, USA, 2015SPE-173633-MS.

[14] W. Qiang, Z. Chaoneng, Z. Jinzhou et al., "Numerical simulation of planar hydraulic fracture propagation with consideration to transition from turbulence to laminar flow regime," *Engineering Fracture Mechanics*, vol. 262, p. 108258, 2022.

[15] Q. Wang, Y. Hu, J. Zhao, S. Chen, C. Fu, and C. Zhao, "Numerical simulation of fracture initiation, propagation and fracture complexity in the presence of multiple perforations," *Journal of Natural Gas Science and Engineering*, vol. 83, article 103486, 2020.

[16] C. Zhao, Q. Wang, J. Zhao et al., "An understanding of oil-water replacement mechanism based on interfacial tension gradient during the well shut-in," *Energy Reports*, vol. 8, pp. 4006–4021, 2022.

[17] Q. Wang, J. Zhao, B. Wang et al., "Secondary growth and closure behavior of planar hydraulic fractures during shut-in," *Journal of Petroleum Science and Engineering*, vol. 213, article 110420, 2022.

[18] J. Zhang, M. He, J. Gu et al., "Rock mass classification for columnar jointed basalt: a case study of Baihetan Hydropower Station," *Geofluids*, vol. 2020, Article ID 6679317, 12 pages, 2020.

[19] Y. Xing, B. Huang, E. Ning, L. Zhao, and F. Jin, "Quasi-static loading rate effects on fracture process zone development of mixed-mode (I-II) fractures in rock-like materials," *Engineering Fracture Mechanics*, vol. 240, p. 107365, 2020.

[20] Y. Xing, B. Huang, and L. Hu, "Injection rate-dependent deflecting propagation rule of hydraulic fracture: insights from the rate-dependent fracture process zone of mixed-mode (I-II) fracturing," *Geofluids*, vol. 2021, Article ID 8199095, 17 pages, 2021.

[21] R. Yang, C. Chen, P. Xu, C. Ding, and Z. Zhang, "Experimental investigation of obliquely incident blast wave effect on deflection of running cracks," *Journal of Testing and Evaluation*, vol. 49, no. 2, pp. 866–880, 2019.

[22] M. Zhai, D. Wang, L. Li et al., "Investigation on the mechanism of hydraulic fracture propagation and fracture geometry control in tight heterogeneous glutenites," *Energy Exploration & Exploitation*, vol. 40, no. 1, pp. 246–278, 2022.

[23] H. Zheng, C. Pu, Y. Wang, and C. Sun, "Experimental and numerical investigation on influence of pore-pressure distribution on multi-fractures propagation in tight sandstone," *Engineering Fracture Mechanics*, vol. 230, p. 106993, 2020.

[24] J. Zhao, J. Zhao, Y. Hu, T. Huang, X. Zhao, and X. Liu, "Non-planar fracture propagation model for fluid-driven fracturing based on fluid-solid coupling," *Engineering Fracture Mechanics*, vol. 235, p. 107159, 2020.

[25] D. Zhou, P. Zheng, P. He, and J. Peng, "Hydraulic fracture propagation direction during volume fracturing in unconventional reservoirs," *Journal of Petroleum Science and Engineering*, vol. 141, pp. 82–89, 2016.

[26] P. Zheng, T. Gu, E. Liu, M. Zhao, and D. Zhou, "Simulation of fracture morphology during sequential fracturing," *PRO*, vol. 10, no. 5, p. 937, 2022.

[27] X. Li, Y. Liang, Y. Luo, and C. Ai, "Predicting hydraulic fracture propagation based on maximum energy release rate theory with consideration of T-stress," *Fuel*, vol. 269, p. 117337, 2020.

[28] D. Zhou, P. Zheng, J. Yang et al., "Optimizing the construction parameters of modified zipper fracs in multiple horizontal wells," *Journal of Natural Gas Science and Engineering*, vol. 71, p. 102966, 2019.

[29] M. Abolghasemzadeh, Y. Alizadeh, and H. Mohammadi, "Fatigue strength reduction factors based on strain energy density applied to sharp and blunt notches under multiaxial loading," *Physical Mesomechanics*, vol. 23, no. 1, pp. 66–80, 2020.

[30] G. Zhang and M. Chen, "Dynamic fracture propagation in hydraulic re-fracturing," *Journal of Petroleum Science and Engineering*, vol. 70, no. 3-4, pp. 266–272, 2010.

[31] J. Geertsma and F. De Klerk, "A rapid method of predicting width and extent of hydraulically induced fractures," *Journal of Petroleum Technology*, vol. 21, no. 12, pp. 1571–1581, 1969.

[32] J.-H. Kim and G. H. Paulino, "On fracture criteria for mixed-mode crack propagation in functionally graded materials," *Mechanics of Advanced Materials and Structures*, vol. 14, no. 4, pp. 227–244, 2007.

[33] W. Cheng, Y. Jin, and M. Chen, "Reactivation mechanism of natural fractures by hydraulic fracturing in naturally fractured shale reservoirs," *Journal of Natural Gas Science & Engineering*, vol. 23, no. part_P3, pp. 431–439, 2015.

[34] S. L. Crouch, "Solution of plane elasticity problems by the displacement discontinuity method. I. Infinite body solution," *International Journal for Numerical Methods in Engineering*, vol. 10, no. 2, pp. 301–343, 1976.

[35] S. L. Crouch, A. M. Starfield, and F. J. Rizzo, *Boundary Element Methods in Solid Mechanics*, vol. 50, Goerge Allen and Unwin Publishers, London, 1983.

[36] P. Zheng, Y. Xia, T. Yao et al., "Formation mechanisms of hydraulic fracture network based on fracture interaction," *Energy*, vol. 243, article 123057, 2022.

[37] K. Wu, *Numerical modeling of complex hydraulic fracture development in unconventional reservoirs, [Ph.D. thesis]*, University of Texas at Austin, 2014.

[38] J. E. Olson, "Fracture aperture, length and pattern geometry development under biaxial loading: a numerical study with applications to natural, cross-jointed systems," *Geological Society, London, Special Publications*, vol. 289, no. 1, pp. 123–142, 2007.

[39] F. Erdogan and G. C. Sih, "On the crack extension in plates under plane loading and transverse shear," *Journal of Basic Engineering*, vol. 85, no. 4, pp. 519–525, 1963.

[40] I. N. Sneddon and H. A. Elliott, "The opening of a Griffith crack under internal pressure," *Quarterly of Applied Mathematics*, vol. 4, no. 3, pp. 262–267, 1946.

[41] A. A. Griffith, "VI. The phenomena of rupture and flow in solids," *Series A, Containing Papers of a Mathematical or Physical Character*, vol. 221, no. 582-593, pp. 163–198, 1921.

[42] P. Valkó and J. Michael, "Economides," in *Hydraulic Fracture Mechanics. Vol. 28*, Wiley, Chichester, 1995.

[43] Y. Yao, W. Wang, and L. M. Keer, "An energy based analytical method to predict the influence of natural fractures on hydraulic fracture propagation," *Engineering Fracture Mechanics*, vol. 189, pp. 232–245, 2018.